International Journal of Heat and Fluid Flow 29 (2008) 1603–1611

Contents lists available at ScienceDirect

International Journal of Heat and Fluid Flow

journal homepage: www.elsevier.com/locate/ijhff

CFD simulations of the effect of inlet conditions on Taylor flow formation

N. Shao, W. Salman, A. Gavriilidis, P. Angeli *

Department of Chemical Engineering, University College London, Torrington Place, London WC1E 7JE, UK

ARTICLE INFO

Article history:
Received 24 June 2007
Received in revised form 11 May 2008
Accepted 27 June 2008
Available online 6 September 2008

Keywords:
Taylor flow
Microchannel
CFD
Inlet conditions
Bubble formation mechanism

ABSTRACT

The mechanism of Taylor bubble formation and the resulting bubble size in capillaries at low superficial gas velocity (U_{GS} < 0.04 m/s) were investigated using Computational Fluid Dynamics (CFD). A co-flow inlet configuration in a 1 mm ID capillary with two gas nozzle sizes of 0.11 mm and 0.34 mm ID, respectively, was studied. Air and three liquids – water, octane and "semi-octane" – were used as test fluids. Bubble formation followed a multi-stage mechanism while the bubble shape during formation deviated from the spherical one assumed in the literature. The three-phase contact line was also found to move along the top wall of the nozzle for the small size nozzle, which had an effect on the bubble size formed. Simulated bubble sizes compared favourably with experimental data in a similar system. Bubble sizes were found to increase with increasing gas and decreasing liquid velocities and increasing nozzle size and nozzle wall thickness. From the fluid properties, surface tension was found to have a strong effect on bubble size but not density or viscosity. An increase in contact angle also increased bubble size. From the available literature correlations those that included phase fraction or ratios of superficial phase velocities were found to predict better the observed bubble sizes.

1. Introduction

As one of the dominant two-phase flow patterns in microchannels, Taylor flow is characterised by periodic occurrence of elongated capsular bubbles with an equivalent diameter several times that of the channel. The bubbles are separated by liquid slugs while only a thin liquid film (usually a very small percentage of the channel diameter) exists between them and the channel wall. Because the liquid phase is interrupted by the bubbles the flow pattern in the liquid slugs is modified to form toroidal vortices, which affect hydrodynamics and mass and heat transfer within the liquid significantly. The primary advantages offered by Taylor flow are the greatly reduced axial (Salman et al., 2004) and improved radial mixing (van Baten and Krishna, 2004), which can augment two- or three-phase reactions (Vandu et al., 2005) or enhance liquid–liquid mixing (Günther et al., 2005). In addition, the diminished channel dimensions in microchannels result in laminar flow which renders the modelling of Taylor bubble systems easier.

A number of investigations have shown that Taylor flow hydrodynamics and mass transfer performance are slug length dependent (Irandoust et al., 1992; Kreutzer, 2003). From inlet gas and liquid flowrates, the slug to bubble length ratio can be determined (Thulasidas et al., 1995). Their absolute values, however, will depend on the dynamics of the two-phase contacting at the inlet. Inlet geometry, fluid physical properties and operating conditions will determine the bubble formation mechanism.

Single bubble formation from gas nozzle or orifice in a pool of Newtonian fluid has been studied by many investigators (for example see Kumar and Kuloor, 1967; Kim et al., 1994; Bhunia et al., 1998; Nahral Henry and Kamotani, 2000; Gnyloskurenko et al., 2003). A force balance analysis during the formation process characterised most of these works and two sets of forces, namely detaching and attaching forces, were identified. Factors affecting bubble formation and corresponding forces as proposed by the literature include gas-flux, buoyancy, bubble inertia, liquid inertia, shear-lift, pressure, surface tension and liquid drag (Kim et al., 1994; Bhunia et al., 1998; Nahral Henry and Kamotani, 2000). Their relevant importance is determined by the scale of the system and the flow regime. For example, the attaching effect of surface tension could be predominant at small scales or reduced gravity, while the effect of liquid drag force could be significantly different in a fast flowing compared to a quiescent liquid. Accordingly, various bubble formation models have been developed and the bubble volume was defined. In the single-stage model of Walters and Davidson (1963), the detaching force was considered to be in a continuous balance with the attaching force. Kumar and Kuloor (1967) disagreed with this static model and proposed a dynamic two-stage model, in which a force balance was only achieved at the end of the first stage. The two stages defined were bubble expansion and detachment. During the expansion stage, bubbles reside on the nozzle while during the detachment stage they "lift off" and form a neck connecting them to the nozzle tip. The two-

* Corresponding author. Tel.: +44 20 7679 3832; fax: +44 20 7383 2348.
E-mail address: p.angeli@ucl.ac.uk (P. Angeli).

0142-727X/$ - see front matter © 2008 Published by Elsevier Inc.
doi:10.1016/j.ijheatfluidflow.2008.06.010

Nomenclature

d	internal or hydraulic diameter, m
$\overline{F}$	dimensionless force term in momentum equation, –
g	gravitational constant, m/s^2
h	height of a rectangular channel, m
L	length, m
p	pressure, kg/ms^2
$\overline{p}$	dimensionless pressure, $p/\rho U_{TP}^2$, –
Q	volumetric flowrate, m^3/s
r	radius, m
t	time, s
$\overline{t}$	dimensionless time, tU_{TP}/d_C, –
u	velocity, m/s
$\overline{u}$	dimensionless velocity, u/U_{TP}, –
U	velocity, m/s
w	width of a rectangular channel, m

Greek symbols

α	a constant of order one, –
ε	volume fraction of fluid, –
μ	dynamic viscosity, Pa s
$\overline{\mu}$	dimensionless dynamic viscosity, –
ρ	density, kg/m^3
$\overline{\rho}$	dimensionless density, –
σ	surface tension, N/m
$\overline{\sigma}$	dimensionless surface tension, –
θ	current contact angle, °

Dimensionless numbers

Ca	capillary number, $\mu_L U_B/\sigma$
Eo	Eötvös number, $(\rho_L - \rho_G)d_C^2 g/\sigma$
Re_B	unit cell Reynolds number, $\rho_L U_B d_C/\mu_L$
Re_G	Reynolds number based on the gas phase, $\rho_G U_{GS} d_C/\mu_G$
Re'_G	Reynolds number in Eq. (15) based on the gas phase superficial velocity, $\rho_L U_{GS} d_C/\mu_L$
Re_L	Reynolds number based on the liquid phase, $\rho_L U_{LS} d_C/\mu_L$

Subscripts

B	bubble
C	channel or capillary
G	gas
GS	gas phase superficial
L	liquid
LS	liquid phase superficial
N	gas nozzle
S	slug
TP	two-phase
UC	unit cell

stage model is frequently adopted for the investigation of bubble formation (Kim et al., 1994; Bhunia et al., 1998; Nahral Henry and Kamotani, 2000). Gnyloskurenko et al. (2003) investigated bubble formation from a 1mm diameter orifice at very low gas flowrates of 2 ml/min (U_{GS} = 0.042 m/s) and presented a multistage model, in which the stages of bubble nucleation, under critical growth, critical growth and necking, were identified.

By equating the detaching and attaching forces, bubble volume can be calculated. At intermediate and low gas flowrates (<10^4 ml/s), the effect of the inertia force diminishes (Kumar and Kuloor, 1967), while the effect of surface tension has to be included to balance the buoyancy force. The fact that the discrepancy between model predictions and experimental data increased with decreasing gas flow rate (Gnyloskurenko et al., 2003) suggests that other parameters, apart from surface tension, play a role. In the study of Byakova et al. (2003), bubble volume at low gas velocity was found to depend on wettability. By increasing the equilibrium contact angle, i.e. worsening the liquid wettability on the gas nozzle wall, the bubble volume was found to increase by more than 50%.

Taylor bubble sizes in microchannels, however, cannot be predicted accurately by models based on force balance. On one hand, Taylor bubbles deform significantly as they grow and approach the channel wall, deviating from the spherical shape assumed by most force balance models. On the other hand, at the low Reynolds numbers encountered in microchannels viscous forces are important and have to be taken into account. Some correlations based on both experimental data and numerical simulations have been suggested in the literature (Table 1). Laborie et al. (1999) correlated experimentally bubble and slug lengths in 1–4 mm capillaries to Reynolds and Eötvös numbers as given by Eqs. (14) and (15), respectively. A porous membrane was used to form the dispersed phase. Based on the experimental data by Heiszwolf et al. (2001) in a 200cpsi monolith reactor, where a distributor was used for the liquid phase, Kreutzer (2003) suggested Eq. (16) for slug length in square channels. Liu et al. (2005) used the dependence of mass transfer coefficient on slug length (Berčic and Pintar, 1997) to derive an empirical correlation (Eq. (17)) from their experiments in capillaries ranging from 0.9 to 3 mm ID and with a T-inlet. The predictions seemed to be good (Fig. 10 in their study), but the comparison with Eqs. (15) and (16) was poor. Eq. (17) was further modified by Akbar and Ghiaasiaan (2006) to include gas holdup (Eq. (18)) by fitting their numerical results and the data by Liu et al. (2005) and Laborie et al. (1999). The agreement was satisfactory with a standard deviation of 19.5%. In another numerical study of Taylor bubble and slug lengths, Qian and Lawal (2006) correlated their 148 set of data obtained by Computational Fluid Dynamics 2D simulations in a microchannel with 1 mm width and T-inlet with different dimensions to derive the length of a unit cell (one bubble and one slug) (Eq. (19)). Bubble and slug lengths can be obtained by multiplying the equation with the respective phase holdup. The correlation showed that the bubble and slug lengths depend mainly on the phase holdup and slightly on Reynolds and Capillary numbers. Garstecki et al. (2006) suggested a scaling law (Eq. (20)) to determine bubble size formed via a T-junction in a rectangular microchannel of width w. The value of α is of the order of 1, depending on the geometry of the T-junction, but is independent of the fluid properties (flow rates and two-phase superficial velocities are between 0.01–1 μl/s, and 0.1–1.1 m/s, respectively). In contrast to Garstecki et al. (2006), Xiong et al. (2007) reported for fluids that joined in parallel at the inlet that viscosity and surface tension affected bubble size and proposed to replace the channel width w in Eq. (20) by bubble width w_B. In their study α was equal to 1. Cubaud et al. (2005), using a cross-flow inlet, also found a correlation similar to Eq. (20) where ε_L^{-1} was used instead of $1 + Q_G/Q_L$ but without the coefficient α.

The above correlations show the dependence of bubble and slug sizes on operating conditions and fluid properties. The lack of agreement between correlations suggests that other parameters also affect the sizes. Qian and Lawal (2006) found significant dependence of bubble and slug lengths on the inlet geometry. By varying T-junction orientation and size of inlet channels as well as the degree of premixing of the two fluids in their numerical simulations, the slug length was found to vary up to 300% under the same operating conditions. In general, small mixing zones and

Table 1
Literature correlations on bubble/slug lengths under Taylor flow

Laborie et al. (1999)	$\frac{L_B}{d_C} = 0.0878\frac{Re_B^{0.63}}{Eo^{1.26}}, \quad Re_B = \frac{\rho_L U_B d_C}{\mu_L}, \quad Eo = \frac{(\rho_L - \rho_G)d_C^2 g}{\sigma}$	(14)
	$\frac{L_S}{d_C} = 3451\left(\frac{1}{Re'_G Eo}\right)^{1.27}, \quad Re'_G = \frac{\rho_L U_{GS} d_C}{\mu_L}$	(15)
Kreutzer (2003)	$\frac{L_S}{d_C} = \frac{\varepsilon_L}{-0.00141 - 1.556\varepsilon_L^2 \ln(\varepsilon_L)}, \quad \varepsilon_L \approx \frac{U_{LS}}{U_{GS} + U_{LS}}$	(16)
Liu et al. (2005)	$\frac{U_{TP}}{\sqrt{L_S}} = 0.088 Re_G^{0.72} Re_L^{0.19*}, \quad Re_G = \frac{\rho_G U_{GS} d_C}{\mu_G}, \quad Re_L = \frac{\rho_L U_{LS} d_C}{\mu_L}$	(17)
Akbar and Ghiaasiaan (2006)	$\frac{U_{TP}^{-0.33}}{\sqrt{L_S}} = 142.6\varepsilon_G^{0.56}\left(\frac{d_C}{L_{UC}}\right)^{0.42} Re_G^{-0.252*}, \quad \varepsilon_G = \frac{U_{GS}}{U_B}$	(18)
Qian and Lawal (2006)	$\frac{L_B + L_S}{d_C} = 1.637\varepsilon_G^{-0.893}(1-\varepsilon_G)^{-1.05} Re_B^{-0.075} Ca^{-0.0687}, \quad \varepsilon_G \approx \frac{U_{GS}}{U_{GS} + U_{LS}}, \quad Ca = \frac{\mu_L U_B}{\sigma}$	(19)
Garstecki et al. (2006)	$\frac{L_B}{w} = 1 + \alpha\frac{Q_G}{Q_L}, \quad Q < 0.06\text{ml/min}, \quad Ca < 10^{-2}$	(20)

*Equation is not dimensionless and units are in SI.

good premixing at the inlet favoured short bubble and slug lengths. Bubble size distributions at constant operating conditions have also been observed, e.g. experimentally by Mantle et al. (2002) and theoretically by Qian and Lawal (2006), who attributed them to the toroidal vortices that are generated at the inlet and propagate throughout the channel length. Kreutzer et al. (2005) bounded the occurrence of uniform slug and bubble sizes to $0.25 < U_{LS}/U_{GS} < 2$.

Systematic experimental investigations on the effect of inlet conditions on Taylor flow were carried out by Amador et al. (2004). Taylor bubble formation was found to follow three mechanisms: formation of a gas chamber at the top of the gas nozzle with the bubble detaching from the end of it; formation of a meniscus at the nozzle that leads to pressure built up behind it until the gas finally erupts to form a bubble; the third mechanism is similar to the two-stage model known in the literature. Bubble lengths, formed at T- and Y-junction and co-flow configurations with various gas/liquid inlet dimensions, were found to depend significantly on the ratio of gas to liquid superficial velocities and gas inlet diameter for any given geometry. According to Garstecki et al. (2006) under typical conditions in microchannels (widths and heights of the order of 10–100 μm, flow rates of the order of 0.01–1 μl/s and $Ca < 10^{-2}$), where interfacial forces dominate shear stresses, bubble break-up is controlled by the pressure drop across the bubble. A "squeezing mechanism" was suggested to describe the process: the expansion of gas phase to the entire cross section of the main channel confines the liquid phase to the film region, and builds up pressure upstream the liquid that leads to the "squeezing" of the bubble neck until complete bubble breakage. However, the model is only appropriate when the width to the height ratio of the main channel is larger than 1 and the gas inlet to the main channel width ratio is larger than 0.5. Bubble size was found to be determined by the ratio of the volumetric flowrates of the two phases and the T-junction geometry (see Eq. (20)), which agreed with Amador et al. (2004). Haverkamp et al. (2006) characterised gas–liquid flow in single and multiple rectangular microchannels by using two inlet mixing geometries. For both of them the gas-feed was flanked by two equal liquid inlets, but the channel connecting to the main channel had different designs. In the T-mixer, the width of the connecting channel followed a two-stage reduction while in the smooth mixer the width of the channel was smoothly reduced. The mixer design was reported to affect the flow pattern map and the bubble formation mechanism. In the smooth mixer bubble sizes were reduced and the bubble size distribution was narrower compared to the T-mixer.

The simple and periodic morphology of Taylor flow and the laminar flow characteristics in microchannels make the system particularly suited for investigations through Computational Fluid Dynamics (CFD) simulations. A number of studies exists on the CFD modelling of hydrodynamics and mass transfer of Taylor bubbles within microcapillaries or channels (see for example Taha and Cui, 2006; van Baten and Krishna, 2004, 2005). In these studies the Taylor bubbles are taken to be fully formed and their lengths are assumed. Qian and Lawal (2006) studied numerically Taylor bubble formation in a microchannel with a T-inlet implementing CFD with the Volume of Fluid (VOF) model. However, coarse grids were used in their study and the thin film surrounding the bubbles was not observed; this could have affected the mechanism of bub-

ble formation and subsequently bubble size. CFD has also been used by Xiong et al. (2007) to study bubble formation in an inlet where the two fluids were joined in a stratified manner.

In this work, CFD modelling is used to study the formation of Taylor bubbles in a capillary with a co-flow inlet configuration. The effect on bubble sizes of inlet conditions such as fluid velocities and gas nozzle size as well as surface tension and wall wetting properties, are investigated. The results are compared with experimental data from a similar system by Amador et al. (2004) and with other literature correlations.

2. Flow systems and model formulation

The formation of Taylor bubbles is investigated in a capillary with 1mm internal diameter and smooth walls. A co-flow configuration is used at the inlet where the gas enters in the centre of the channel via a nozzle while the liquid flows around the nozzle as an annulus. The range of nozzle sizes and the inlet conditions investigated are summarised in Table 2.

Air is selected as the gas phase and paired with three different liquid phases, water, octane and "semi-octane", whose physical properties are listed in Table 3. Semi-octane is a hypothetical fluid used for the simulation, that has the same density and viscosity as water, but its surface tension is that of octane. It is used to isolate the effect of surface tension on the bubble formation mechanism.

The CFD software CFX 4.3 (by ANSYS) is used for the simulations, which employs the VOF model for tracking the gas–liquid interface. The main advantage of VOF, compared to other front capturing methods, is its inherent volume conserving nature; this provides a good base to compare the simulated bubble volumes formed at the inlet with those measured experimentally (Amador et al., 2004). The model assumes negligible effects of gravity, surface tension gradient (Marangoni effect) and gas compressibility. The transport equations are discretised by the finite volume method, applying a 'HYBRID' differencing scheme while pressure and velocity are coupled using the SIMPLEC algorithm. Surface tension is included as an extra body force in the momentum equation via the Continuum Surface Force (CSF) model. A very small time step ($1E-4\bar{t}$) is used to allow frequent interface profile modifications through a surface sharpening algorithm. At the wall, the interface normal and the interface curvature are modified according to the contact angle given. The solution domain and its boundary conditions are depicted in Fig. 1. The solution domain is constructed as a two-dimensional axisymmetric geometry in cylindrical coordinates, consisting of a main channel (right hand block in Fig. 1) with a length three times that of the channel diameter and a gas nozzle (left hand block in Fig. 1) with various widths but constant length of $0.3d_C$. No-slip boundary condition is applied to all wall areas, highlighted in Fig. 1 by the hatched pattern. Close to the wall region of the main channel the grid is refined so that the liquid film between the Taylor bubble and the wall can be obtained. The grid sensitivity study was carried out by monitoring the velocity term along the symmetry axis, and the number of computational cells was determined to be around 2×10^4.

The simulations were performed in an IBM RS/6000 workstation with Power 3 II processor, and the average running time for each case was approximately five days.

The governing equations are momentum balance (Eq. (1)) and continuity equation (Eq. (2)), where $\overline{u}$, $\overline{p}$, $\overline{t}$ and $\overline{F}$ are dimensionless velocity vector, pressure, time and a body force term respectively. When a control volume is not entirely occupied by one phase, mixture properties are applied as shown in Eqs. (3) and (4). The density $\overline{\rho}$ and viscosity $\overline{\mu}$ are found from the volume fraction weighted averages of the respective single phase properties. For two-phase flow problems, the volume fraction of one phase is tracked by solving a phase marker function Eq. (5) and that of the other is derived from Eq. (6). All equations have been non-dimensionalised using as reference length the capillary diameter, d_C; reference velocity the two-phase average velocity in the capillary, U_{TP}; and reference time t, the ratio d_C/U_{TP}. The fluid properties in dimensionless form are given in Eqs. (7)–(11).

$$\frac{\partial(\overline{\rho u})}{\partial \bar{t}} + \overline{\nabla} \cdot (\overline{\rho u u}) + \overline{\nabla}\overline{p} = \overline{\nabla} \cdot [\overline{\mu}(\overline{\nabla}\overline{u} + \overline{\nabla}\overline{u}^{T})] + \overline{F}, \tag{1}$$

$$\frac{\partial \overline{\rho}}{\partial \bar{t}} + \overline{\nabla} \cdot (\overline{\rho u}) = 0, \tag{2}$$

$$\overline{\rho} = \overline{\rho}_G \varepsilon_G + \overline{\rho}_L \varepsilon_L, \tag{3}$$

$$\overline{\mu} = \overline{\mu}_G \varepsilon_G + \overline{\mu}_L \varepsilon_L, \tag{4}$$

$$\frac{\partial \varepsilon_G}{\partial \bar{t}} + \overline{u} \cdot \overline{\nabla} \varepsilon_G = 0, \tag{5}$$

$$\varepsilon_G + \varepsilon_L = 1, \tag{6}$$

$$\overline{\rho}_G = \frac{\rho_G U_{TP} d_C}{\mu_L}, \tag{7}$$

$$\overline{\mu}_G = \frac{\mu_G}{\mu_L}, \tag{8}$$

$$\overline{\rho}_L = \frac{\rho_L U_{TP} d_C}{\mu_L}, \tag{9}$$

$$\overline{\mu}_L = \frac{\mu_L}{\mu_L} = 1, \tag{10}$$

$$\overline{\sigma} = \frac{\sigma}{\mu_L U_{TP}}. \tag{11}$$

Table 2
Values of parameters used in the simulations

Inlet conditions	Value/value range
Fluid pair	Air/water; air/octane; air/semi-octane
Gas nozzle size (ID/OD)	0.11/0.21 mm; 0.34/0.64 mm
Gas superficial velocity U_{GS}	0.01–0.033 m/s
Liquid superficial velocity U_{LS}	0.01–0.02 m/s
Contact angle	0°; 60°; 180°

Table 3
Properties of fluids used in the simulations

Fluid	ρ (kg/m^3)	μ (Pa s)	σ (N/m)
Air	1.19	1.7×10^{-5}	–
Water	998	0.001	0.07226
Octane	703	0.00052	0.02149
Semi-octane	998	0.001	0.02149

3. Results and discussion

3.1. Bubble formation mechanism

Bubble formation in the small gas nozzle (0.11 mm ID) for the air–water system is depicted in Fig. 2 and Fig. 3 for two extreme scenarios: $\theta = 0°$ and $\theta = 180°$. A multistage mechanism that consists of the expanding, contracting and necking stages is observed; these descriptions refer to the movement of the gas–liquid interface at the lower end of the bubble close to the nozzle. In the initial expanding stage (Figs. 2A–C and 3A–C) the liquid is displaced by the emerging gas while the gas–liquid interface moves away from the tube central axis. As the bubble is pushed forward in the channel, the interface retracts back towards the central axis (contracting stage, Figs. 2D and 3D–E). It is the expanding and contracting stages that contribute mostly to the bubble volume. As the bubble grows further in the radial direction and starts blocking the channel leaving only a thin liquid film close to the wall, liquid pressure

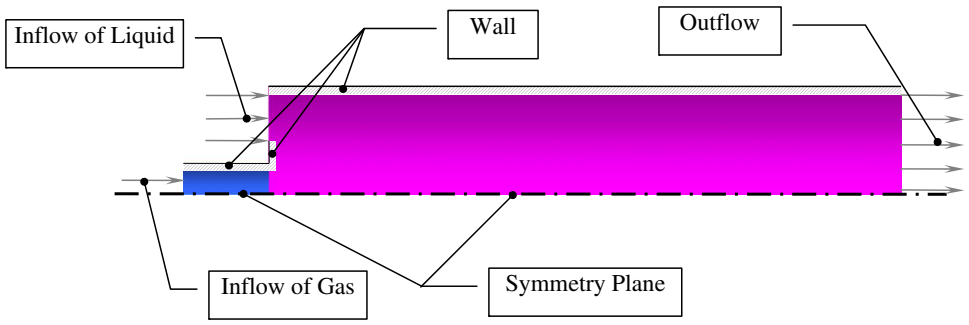

Fig. 1. The solution domain with its boundary conditions.

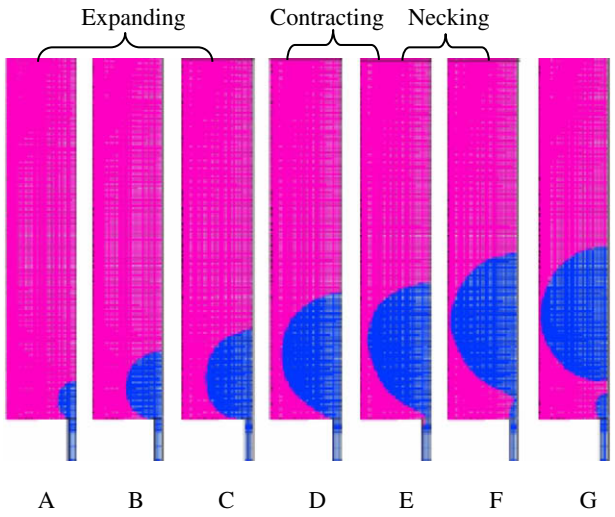

Fig. 2. Bubble formation process for air–water system: $U_{GS} = 0.0155$ m/s, $U_{LS} = 0.02$ m/s, $d_N = 0.11$ mm, $\theta = 0°$ at times A: 0.0014 s, B: 0.007 s, C: 0.014 s, D: 0.028 s, E: 0.0322 s, F: 0.0378 s and G: 0.0392 s.

builds up upstream. The lower end of the bubble is squeezed and as a result a neck forms that connects the bubble body with the tip of the gas nozzle (Figs. 2E and F and 3E). This is the necking stage, which takes place quickly in only several hundred time steps or less (e.g. 0.007 s in Fig. 2) compared with several thousand time steps needed for the previous stages (e.g. 0.032 s in Fig. 2). Finally the neck pinches off and the bubble moves downstream (Figs. 2G and 3F). During these stages, the bubble shape changes. When gas phase first emerges, the bubble assumes a spherical shape as it is still away from the side channel wall (Figs. 2A and B, and 3A and B). As it expands, the middle part of the bubble grows quickly in the radial direction and forms a spherical zone, which has a smaller diameter than the spherical segment at the top (Figs. 2C and 3C). At the end of the contracting stage, the lower part of the bubble lifts gradually and takes the shape of a truncated cone with the apex in contact with the nozzle (see Fig. 3E). In the case of $\theta = 180°$, gas is now the wetting phase and spreads to the wall to become the continuous phase as soon as the bubble forms (Fig. 3G).

During bubble formation for both contact angles studied, the expanding and contracting stages are accompanied by a movement of the three phase contact line along the top nozzle wall. The results of the current study, in accordance to the observations by Gnyloskurenko et al. (2003), suggest that the three phase contact line moves as shown schematically in Fig. 4. At Position 1 the meniscus is at the inner wall of the nozzle with current contact angle θ. With increasing gas pressure, if there is contact angle hysteresis, the contact angle will change to acquire its receding value before the three phase contact line slides towards the outer nozzle

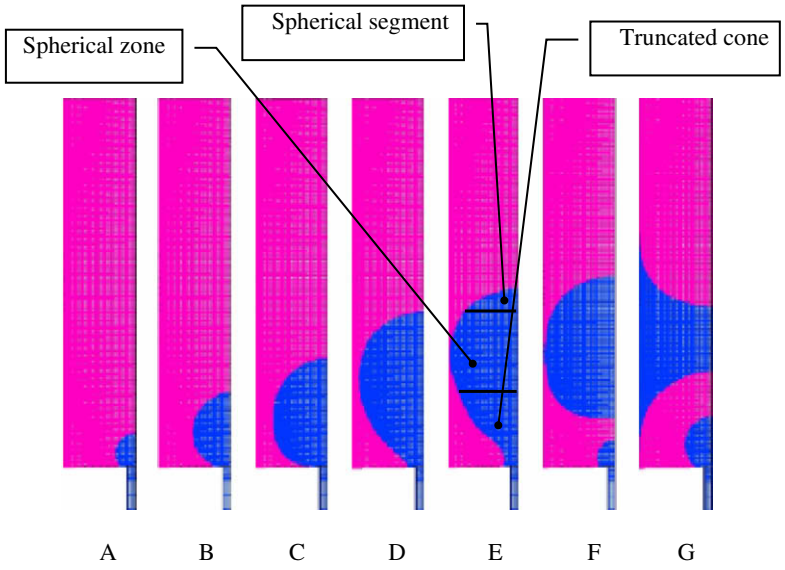

Fig. 3. Bubble formation process for air–water system: $U_{GS} = 0.0155$ m/s, $U_{LS} = 0.02$ m/s, $d_N = 0.11$ mm, $\theta = 180°$ at times A: 0.0014 s, B: 0.007 s, C: 0.021 s, D: 0.035 s, E: 0.0406 s, F: 0.0434 s, and G: 0.0462 s.

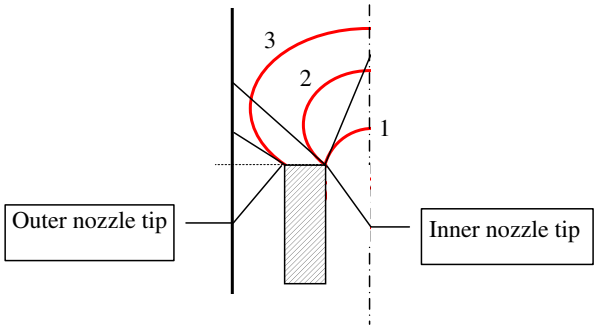

Fig. 4. The movement of the three phase contact line on the top wall of the nozzle during bubble formation at very low gas flowrates.

wall (from position 2 to position 3). As the bubble expands, liquid builds up behind it and the liquid pressure becomes higher than the gas pressure. This pressure difference would resist further movement of the contact line towards the outer nozzle wall. When the contact angle attains its advancing value (if that is different from the equilibrium one), the movement of the contact line will be reversed, i.e. from the outer towards the inner nozzle wall. As seen from Figs. 2 and 3, the movement of the contact line depends on the wetting conditions of the system. In the case of $\theta = 180°$, the complete movement of the contact line (position 2 to position 3 and to position 2 again) occurs after 0.04 s, slower than that in the case of $\theta = 0°$, which is within 0.028 s. As a result, the base of the forming bubble has a wider periphery for longer time in the less wetting case while all other operating conditions are the same.

No contact line movement along the nozzle wall was observed with the large nozzle size, $d_N = 0.34$ mm, at the stored time intervals. This is perhaps because, the larger nozzle size reduces the pressure difference between the gas and the liquid at the contact point, according to Laplace equation (Eq. (12)) and this pressure difference may not be sufficient to initiate movement of the contact line

$$p_G - p_L = \frac{\sigma}{2r}, \tag{12}$$

where p_G and p_L are the pressures at the gas and liquid side, respectively, and $2r = d_N$ at the contact point.

In addition, the larger nozzle size increases the liquid phase inlet velocity for the same flowrate which, because of drag force, would cause the bubble to move downstream faster than in the case of small nozzle. All these contribute to the disappearance of contact line movement within the time interval used.

3.2. Effect of inlet conditions on bubble size

Bubble length is often used in the literature to compare bubble sizes during Taylor flow. It was seen that, because of changes in the bubble shape, the length of the bubbles just after their formation is not constant and would not be representative of their size. To compare with experiments the formed bubble volume is used instead. The use of the VOF model and interface tracking, means that the CFD simulations are computationally very expensive. In order to reduce computational time, the formation of only one or two Taylor bubbles was modelled for each case.

3.2.1. Effect of gas and liquid velocities

As can be seen from Figs. 5 and 6 the bubble volume increases with increasing gas and decreasing liquid superficial velocity respectively. The results also agree very well with experimental data obtained in a system identical to that used in the simulations (Amador et al., 2004). By increasing U_{GS}, the rate that the gas enters

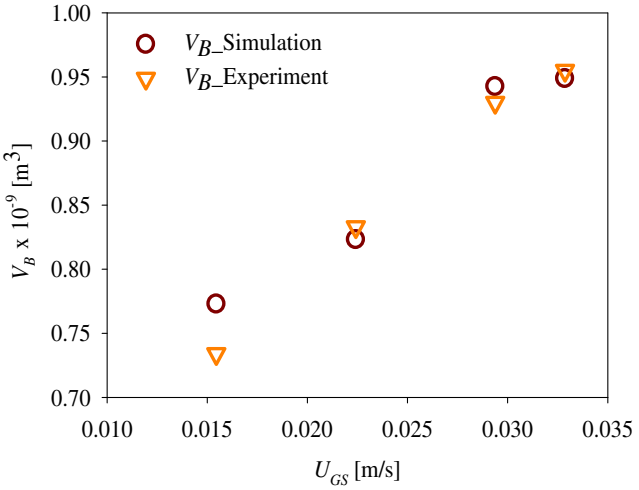

Fig. 5. Simulated and experimental bubble volumes under different gas superficial velocities: air–water system, $U_{LS} = 0.02$ m/s, $d_N = 0.11$ mm, $\theta = 0°$.

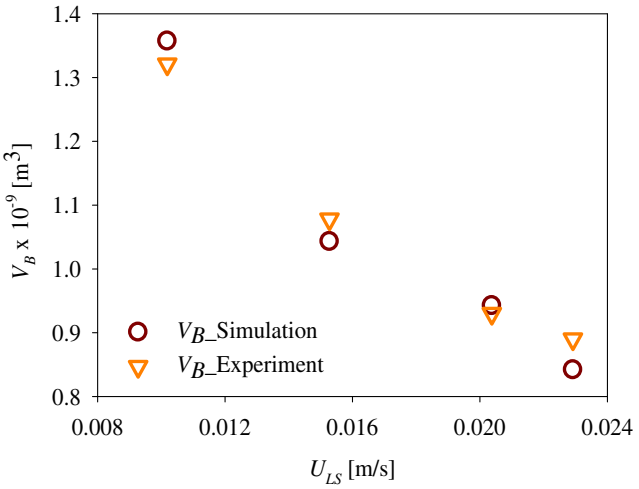

Fig. 6. Simulated and experimental bubble volumes under different liquid superficial velocities: air–water system, $U_{GS} = 0.0294$ m/s, $d_N = 0.11$ mm, $\theta = 0°$.

the forming bubble increases. Although the detaching effect of the gas momentum flux would also increase and shorten the bubble formation time, it is compensated by the faster gas injection rate. With increasing U_{LS}, the detaching effect of liquid drag force increases, and smaller bubbles are formed.

3.2.2. Effect of liquid properties

Three liquid phases, water, octane and semi-octane are used here to study the dependence of bubble sizes on surface tension, density and viscosity of the liquid phase. Fig. 7 shows that the volume of bubbles produced in the octane system is smaller than that in the water system under the same conditions. In semi-octane, which has the density and viscosity of water but the surface tension of octane (Table 3), the bubble volumes are almost the same as those obtained in octane. This suggests that bubble size is mainly affected by surface tension and only slightly by density and viscosity. Compared to water, in octane the reduced attaching effect of the surface tension force causes the bubbles to detach earlier and smaller bubbles form. Both Laborie et al. (1999) and Qian and Lawal (2006) also found that increase in surface tension increased slightly bubble size while viscosity had almost no influence.

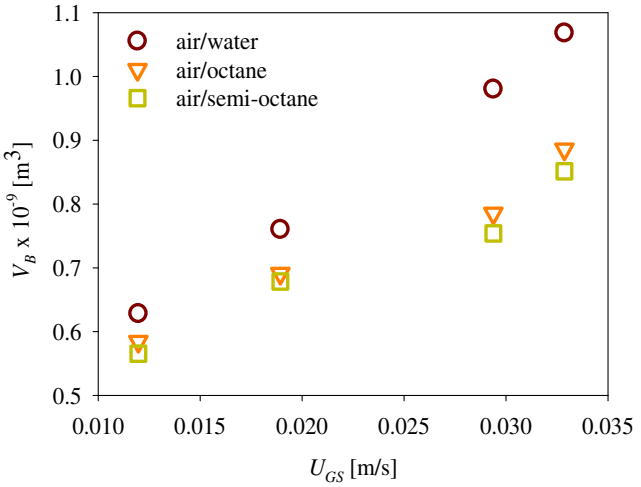

Fig. 7. Simulated bubble volumes for different fluid pairs: U_{LS} = 0.02 m/s, d_N = 0.34 mm, θ = 0°.

3.2.3. Effect of nozzle size and its wall thickness

As can be seen from Fig. 8, increasing the nozzle size from 0.11 mm to 0.34 mm results in an increase in bubble volume. The nozzle size can affect bubble formation in two ways: for the same gas flowrate the gas flux in the large nozzle, which has a detaching effect, decreases; in addition, the increased periphery of the large nozzle increases the surface tension force which has an attaching effect. Both help to extend the bubble formation time and thus its size. Apart from the nozzle size, its wall thickness also seems to play a role on bubble size, as can be seen from Fig. 9, where larger bubbles are observed for the thicker wall. As discussed before, the three-phase contact line can recede and advance along the top nozzle wall during bubble formation. Therefore, for a thicker wall more time is taken by the contact line to move outwards and inwards on the nozzle wall which allows extra time for the bubble to grow. However, when there is no contact line movement along the nozzle wall as in the case of d_N = 0.34 mm, the effect of nozzle wall thickness will probably be absent.

3.2.4. Effect of wetting conditions

To investigate the effect of wetting conditions on bubble size, three equilibrium contact angles are examined for the air–water system (Table 2). From Fig. 10 it can be seen that as the wettability of the liquid worsens, i.e. equilibrium contact angle changes from 0° to 60°, bubble size increases by 7.2% (Fig. 10a and b, respectively). It can also be seen that at time t = 0.03 s, under the same operating conditions, when the first bubble has already detached for θ = 0° and θ = 60°, it is still attached to the gas nozzle for θ = 180°, indicating that a larger bubble size will eventually form. Contact angle would affect the movement of the three phase contact line on the top wall of the nozzle as well as the shape of the gas–liquid interface at the inlet and consequently the amount of gas entering the bubble. These results agree with the experimental observations by Byakova et al. (2003) but are opposite to the numerical predictions of Qian and Lawal (2006). In the latter, no liquid film around the bubble was observed and a three phase contact line existed on the capillary wall downstream of the inlet. As a result, the gas–liquid interface shape changed from concave to convex on the liquid side when θ changed from 0° to 180°; this change in shape affected the measured bubble length which was found to be inversely proportional to θ when the liquid phase was wetting the wall but proportional to it for a non-wetting liquid.

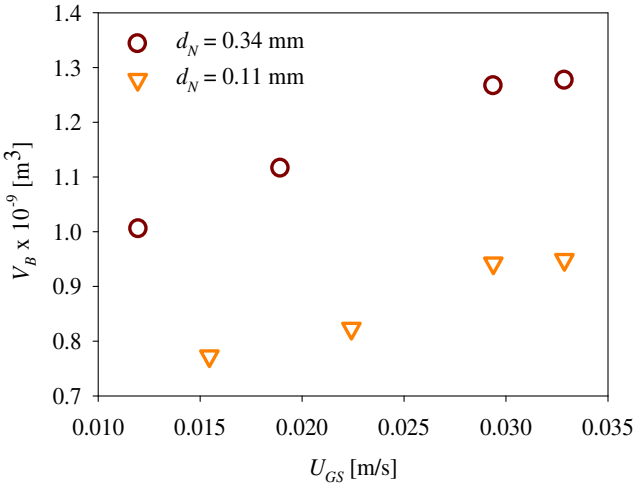

Fig. 8. Effect of gas nozzle size on bubble volume for air–water system, U_{LS} = 0.02 m/s, θ = 0°.

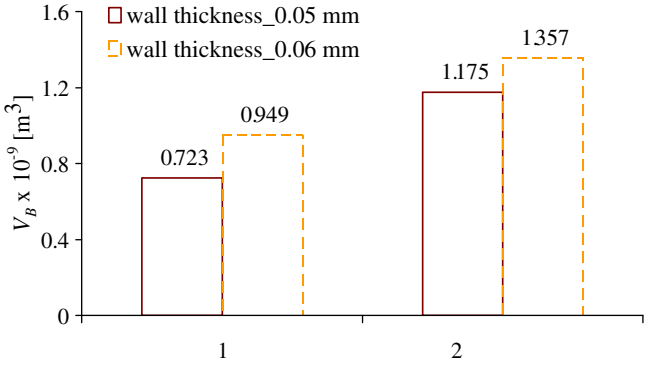

Fig. 9. Effect of wall thickness on bubble volume for air–water system: d_N = 0.11 mm, θ = 0°; (1) U_{GS} = 0.0329 m/s, U_{LS} = 0.02 m/s and (2) U_{GS} = 0.0294 m/s, U_{LS} = 0.01 m/s.

3.3. Comparison of numerical Taylor bubble sizes with literature correlations

As shown in Section 3.2 and also demonstrated in the literature, the geometry of the inlet plays a significant role on the size of the formed bubbles and slugs. A number of correlations have been suggested in the literature for predicting sizes in Taylor flow (Table 1) that use various inlets (see Table 4). Even when T-junctions are

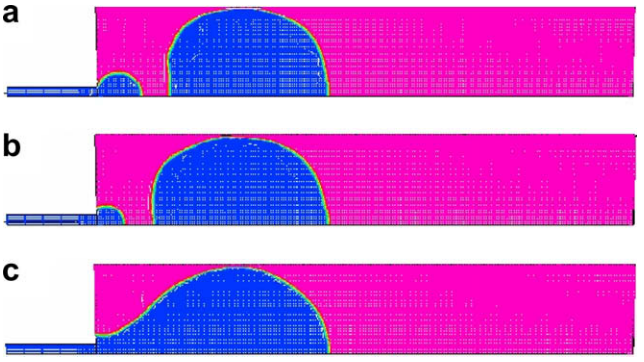

Fig. 10. Bubble formation at t = 0.03 s for different contact angles: (a) θ = 0°, V_B = 0.773 × 10^{-9} m^3; (b) θ = 60°, V_B = 0.829 × 10^{-9} m^3; (c) θ = 180°. d_N = 0.11 mm, U_{GS} = 0.0155 m/s, U_{LS} = 0.02 m/s.

Table 4
Conditions used in literature and in this work for determining bubble length

Literature	Main channel dimension (mm)	Superficial velocities (m/s)	Gas–liquid inlet
Kreutzer (2003)	1.56	$U_{GS} + U_{LS} < 0.75$	Liquid distributor
Garstecki et al. (2006)	h: 0.033, w: 0.05–0.2	U_{GS}: 0.044–0.61, U_{LS}: 0.063–0.51	T-junction
Qian and Lawal (2006)	1	U_{GS}: 0.01–0.25, U_{LS}: 0.01–0.25	T-junction
Laborie et al. (1999)	1–4	U_{GS}: 0.1–0.74, U_{LS}: 0.1–1	Porous membrane
Liu et al. (2005)	0.9–3	U_{GS}: 0.008–0.7, U_{LS}: 0.008–0.5	PVC T-connection
Akbar and Ghiaasiaan (2006)	0.1–1	$0.5 < U_{GS} + U_{LS} < 1.6$	No inlet given
This work	1	U_{GS}: 0.01–0.033, U_{LS}: 0.01–0.02	Co-flow annular configuration

used, the dimensions of the side inlet channels and the angles they join the main channel are not consistent. As such the correlations would only be able to predict sizes in the particular systems they were derived from. Despite these differences, however, the simulated data are compared in this section with the currently available literature correlations shown in Table 1 in order to evaluate their generality and ability to predict bubble/slug sizes during Taylor flow in microchannels.

For the comparison, the Taylor bubble lengths from this study are needed and these were obtained by measuring the axial distance between the front and the rear of the bubble. The comparisons with the literature correlations are depicted in Fig. 11. When only a correlation for the slug length is given, this is transformed to bubble length via Eq. (13) according to Liu et al. (2005). The gas fraction term ε_G is in each case estimated as suggested by the respective author.

$$L_B = L_{UC}\varepsilon_G = \frac{L_S}{\varepsilon_L}\varepsilon_G = \frac{L_S}{(1-\varepsilon_G)}\varepsilon_G. \quad (13)$$

As can be seen in Fig. 11, Eqs. (16) and (20) (with $\alpha = 0.57$ which fitted the data better than $\alpha = 1$) predict well the current data, but all others overpredict them. Apart from the different inlet configurations, another reason for the discrepancy could be the wider range and larger values of channel size and superficial gas and liquid velocities (wide range of Ca) used in the literature than in the current study (Table 4). The model by Garstecki et al. (2006) that predicts the data well, was developed particularly for low Ca, as those encountered in the present study. Furthermore, it is interesting, that the agreement is better with those correlations where volume fraction is included (Kreutzer, 2003; Qian and Lawal, 2006; Garstecki et al., 2006). This would imply that the bubble length is affected by the gas/liquid flowate or velocity ratio ($\varepsilon_L^{-1} \approx 1 + U_{GS}/U_{LS}$ from the definition of liquid volume fraction) more than by the other parameters. When Liu et al. (2005) and Laborie et al. (1999) used the two velocities separately, e.g. expressed in Re_G and Re_L, rather than as a ratio, larger deviation was observed. Interestingly, the correlation by Qian and Lawal (2006) that contains the volume fraction and was derived for velocity ranges and channel size very similar to those used here, still overpredicts the data, despite slightly. Apart from the inlet configurations this discrepancy could also be due to the ratio of gas inlet to main channel used. This ratio was one in the study by Qian and Lawal (2006) but is about 1/9 in the present study. It was discussed in Section 3.2.3 that by increasing the gas inlet size larger bubbles are produced.

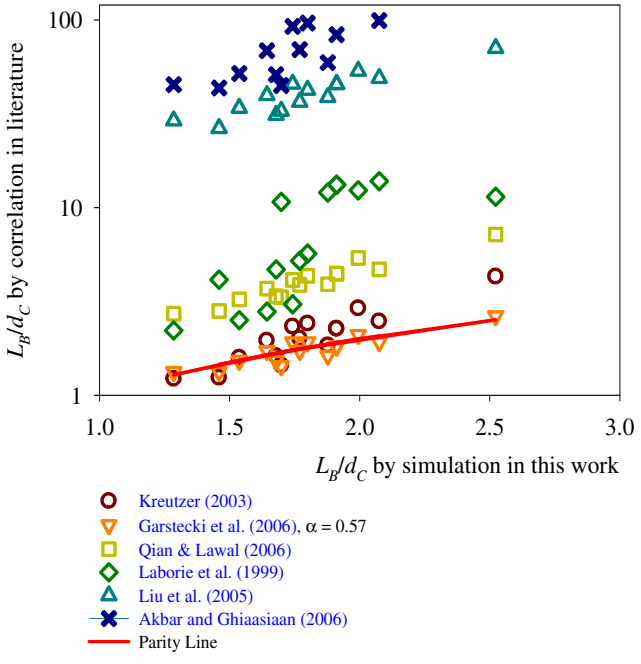

Fig. 11. Comparison of simulated dimensionless bubble lengths with predictions of literature correlations.

4. Conclusions

The mechanism of Taylor bubble formation at the inlet of a microchannel and the ensuing bubble size were studied for very low superficial gas velocities ($U_{GS} < 0.04$ m/s) using CFD modelling. The effect of gas and liquid velocities, liquid properties, contact angle, gas nozzle size and its wall thickness were examined. The results agreed well with experimental data and qualitatively with theoretical considerations from the balance of forces on the forming bubble. It was found that bubble formation follows three stages, namely expanding, contracting and necking. The first two stages that correspond respectively to outward and inward movement of the gas–liquid interface close to the nozzle contribute mostly to bubble size. For the smaller gas nozzle size used, $d_N = 0.11$ mm, the three phase contact line was found to slide along the top of the nozzle wall outwards and inwards during the expanding and contracting stages, respectively. This was not observed for the large nozzle used ($d_N = 0.34$ mm). The bubble shape deviated from spherical for most of the bubble formation time.

It was found that increasing the gas or decreasing the liquid velocity increases the bubble size. Surface tension is found to have a greater effect on bubble size than viscosity and density. Large nozzle size as well as large contact angles favour the formation of larger bubbles. In the case of the small nozzle, increased nozzle thickness was also found to produce larger bubbles.

The bubble sizes found numerically agreed better with those literature correlations that included phase fraction or ratios of superficial phase velocities. The inlet contacting configuration, e.g. the sizes of the inlet channels and the contacting angle of the two phases, which have been found to affect bubble size, are not taken into account in the correlations and would contribute to the discrepancies observed.

Further studies that cover a wider range of properties and inlet conditions would be needed to develop a predictive model for Tay-

lor bubble size in microchannels. The behaviour of the three phase contact line on the gas nozzle needs also further consideration.

Acknowledgements

N. Shao would like to thank the Overseas Research Students Awards Scheme (Universities UK) and the UCL Graduate School for providing financial support for the studentship.

References

Akbar, M.K., Ghiaasiaan, S.M., 2006. Simulation of Taylor flow in capillaries based on the volume-of-fluid technique. Ind. Eng. Chem. Res. 45, 5396–5403.

Amador, C., Salman, W., Sanguanpiyapan, S., Gavriilidis, A., Angeli, P., 2004. Effect of gas-inlet conditions on the mechanism of Taylor flow formation. ICMF'04, Report SP-515, Yokohama.

Berčic, G., Pintar, A., 1997. The role of gas bubbles and liquid slug lengths on mass transport in the Taylor flow through capillaries. Chem. Eng. Sci. 52, 3709–3719.

Bhunia, A., Pais, S.C., Kamotani, Y., Kim, I.H., 1998. Bubble formation in a coflow configuration in normal and reduced gravity. AIChE J. 44, 1495–1509.

Byakova, A.V., Gnyloskurenko, S.V., Nakamura, T., Raychenko, O.I., 2003. Influence of wetting conditions on bubble formation at orifice in an inviscid liquid: mechanism of bubble evolution. Colloid. Surf. A 229, 19–32.

Cubaud, T., Tatineni, M., Zhong, X., Ho, C-M., 2005. Bubble dispenser in microfluidic devices. Phys. Rev. E 72, 037302.

Garstecki, P., Fuerstman, M.J., Stone, H.A., Whitesides, G.M., 2006. Formation of droplets and bubbles in a microfluidic T-junction – scaling and mechanism of break-up. Lab on a Chip 6, 437–446.

Gnyloskurenko, S.V., Byakova, A.V., Raychenko, O.I., Nakamura, T., 2003. Influence of wetting conditions on bubble formation at orifice in an inviscid liquid. Transformation of bubble shape and size. Colloid. Surf. A 218, 73–87.

Günther, A., Jhunjhunwala, M., Thalmann, M., Schmidt, M.A., Jensen, K.F., 2005. Micromixing of miscible liquids in segmented gas–liquid flow. Langmuir 21, 1547–1555.

Haverkamp, V., Hessel, V., Löwe, H., Menges, G., Warnier, M.J.F., Rebrov, E.V., de Croon, M.H.J.M., Schouten, J.C., Liauw, M.A., 2006. Hydrodynamics and mixer-induced bubble formation in micro bubble columns with single and multiple-channels. Chem. Eng. Technol. 29 (9), 1–13.

Heiszwolf, J.J., Engelvaart, L.B., van der Eijnden, M.G., Kreutzer, M.T., Kapteijn, F., Moulijn, J.A., 2001. Hydrodynamic aspects of the monolith loop reactor. Chem. Eng. Sci. 56 (3), 805–812.

Irandoust, S., Ertle, S., Andersson, B., 1992. Gas liquid mass transfer of Taylor flow through a capillary. Can. J. Chem. Eng. 70, 115.

Kim, I., Kamotani, Y., Ostrach, S., 1994. Modelling bubble and drop formation in flowing liquids in microgravity. AIChE J. 40, 19–28.

Kumar, R., Kuloor, N.R., 1967. Chem. Technol. 19, 733.

Kreutzer, M., 2003. Hydrodynamics of Taylor Flow in Capillaries and Monolith Reactors. Delft University Press, Delft.

Kreutzer, M.T., Kapteijn, F., Moulijn, J.A., Kleijn, C.R., Heiszwolf, J.J., 2005. Inertial and interfacial effects on pressure drop of Taylor flow in capillaries. AIChE J. 51, 2428–2440.

Laborie, S., Cabassud, C., Durand-Bourlier, L., Laine, J.M., 1999. Characterization of gas–liquid two-phase flow inside capillaries. Chem. Eng. Sci. 54 (23), 5723–5735.

Liu, H., Vando, C.O., Krishna, R., 2005. Hydrodynamics of Taylor flow in vertical capillaries: flow regimes, bubble rise velocity, liquid slug length, and pressure drop. Ind. Eng. Chem. Res. 44, 4884–4897.

Mantle, M.D., Sederman, A.J., Gladden, L.F., 2002. Dynamic MRI visualization of two-phase flow in a ceramic monolith. AIChE J. 48, 909–912.

Nahral Henry, K., Kamotani, Y., 2000. Bubble formation from wall orifice in liquid cross-flow under low gravity. Chem. Eng. Sci. 55, 4653–4665.

Qian, D., Lawal, A., 2006. Numerical study on gas and liquid slugs for Taylor flow in a T-junction microchannel. Chem. Eng. Sci. 61, 7609–7625.

Salman, W., Gavriilidis, A., Angeli, P., 2004. A model for predicting axial mixing during gas–liquid Taylor flow in microchannels at low Bodenstein numbers. Chem. Eng. J. 101 (1–3), 391–396.

Taha, T., Cui, Z.F., 2006. CFD modelling of slug flow inside square capillaries. Chem. Eng. Sci. 61, 665–675.

Thulasidas, T.C., Abraham, M.A., Cerro, R.L., 1995. Bubble-train flow in capillaries of circular and square cross section. Chem. Eng. Sci. 50 (2), 183–199.

van Baten, J.M., Krishna, R., 2004. CFD simulations of mass transfer from Taylor bubbles rising in circular capillaries. Chem. Eng. Sci. 59, 2535–2545.

van Baten, J.M., Krishna, R., 2005. CFD simulations of wall mass transfer for Taylor flow in circular capillaries. Chem. Eng. Sci. 60, 1117–1126.

Vandu, C.O., Ellenberger, J., Krishna, R., 2005. Hydrodynamics and mass transfer in an upflow monolith loop reactor. Chem. Eng. Process. 44 (3), 363–374.

Walters, J.K., Davidson, J.F., 1963. The initial motion of a gas bubble formed in an inviscid liquid, Part 2. The three-dimensional bubble and the toroidal bubble. Fluid Mech. 17, 321–336.

Xiong, R., Bai, M., Chung, J.N., 2007. Formation of bubbles in a simple co-flowing micro-channel. J. Micromech. Microeng. 17, 1002–1011.